February 2, 2008

The high-intensity hyperon beam at CERN

Yu.A.Alexandrov[1], M.Clement[2], F.Dropmann[3], A.Fournier[4] P.Grafström.[2], E.Hubbard[3], S.Paul[3,a], H.W.Siebert[5], A.Trombini[3] M.Zavertiaev[1]

[1]*Moscow Lebedev Physics Inst., RU-117924, Moscow, Russia.*
[2]*CERN; CH-1211 Genève 23, Switzerland.*
[3]*Heidelberg Max-Planck-Inst. für Kernphysik[#]; Postfach 103980, D-69029 Heidelberg, Germany.*
[4]*Grenoble ISN; 53 Avenue des Martyrs ; F-38026 Grenoble CEDEX, France*
[5]*Heidelberg, Univ., Physikal. Inst.[#]; Philosophenweg 12, D-69120 Heidelberg, Germany.*

Abstract

A high-intensity hyperon beam was constructed at CERN to deliver Σ^- to experiment WA89 at the Omega facility and operated from 1989 to 1994. The setup allowed rapid changeover between hyperon and conventional hadron beam configurations. The beam provided a Σ^- flux of 1.4×10^5 per burst at mean momenta between 330 and 345 GeV/c produced by about 3×10^{10} protons of 450 GeV/c . At the experiment target the beam had a Σ^-/π^- ratio close to 0.4 and a size of 1.6 $\times$ 3.7 cm^2. The beam particle trajectories and their momenta were measured with a scintillating fibre hodoscope in the beam channel and a silicon microstrip detector at the exit of the channel. A fast transition radiation detector was used to identify the pion component of the beam.

(Submitted to Nuclear Instruments and Methods A)

---

a) Now at now at Technische Universität München,Graching, Germany

#) supported by the Bundesministerium für Bildung, Wissenschaft Forschung und Technologie, Germany, under con-

1 Introduction

Our present experimental knowledge of the properties and interactions of hyperons comes mainly from hyperon beam experiments. In contrast to normal hadron beam lines, hyperon beams are characterized by very short lengths of order 10m, which represent a compromise between the need for adequate shielding between the primary hyperon production target and the experimental apparatus and the need to reduce decay losses of the hyperons passing along the beam line. At a momentum of 100 GeV/c, the hyperon decay lengths vary from 7.1m for Λ to 1.5m for Ω^-, which leads to severe reductions of the hyperon fluxes available for experiments. This has induced a continuous quest for higher hyperon beam momenta, which started at about 25 GeV/c at the Brookhaven AGS and the CERN PS in the early seventies. The advent of the super proton synchrotrons at CERN and at FERMILAB in the mid-seventies led to the immediate construction of new hyperon beam lines to exploit the newly available high energies.

At CERN, a charged hyperon beam with momenta between 70 and 135 GeV/c was operated between 1976 and 1982 in the CERN West Hall. It achieved fluxes of 12,000 Σ^-, 400 Ξ^- and 10 Ω^- per beam pulse, all of which were successfully used in experiments. For reviews of these activities see [1] and [2].

The quest for higher Σ^- fluxes then led to the construction of a new hyperon beam line at CERN, capable of delivering in excess of 10^5 Σ^- per beam pulse at 340 GeV/c to the Omega spectrometer facility in the West Hall. The beam was brought into operation in 1989-90 and was used for physics runs in 1991, 1993 and 1994. The design and operation of the beam are the subject of this article.

At FERMILAB the development of hyperon beams culminated in a 600 GeV/c beam delivering Σ^- to the SELEX experiment in 1997 [3].

2 Design considerations

2.1 Boundary conditions

Budget and manpower restrictions led to the decision to base the hyperon beam experiment WA89 on the existing Omega spectrometer facility in the CERN West Area [4], which was used by several different experiments each year. This imposed quite severe restrictions on the design of the beam, which are listed below:

- The Omega spectrometer was situated at the end of the H1 beam line in the West Area. H1 is a high energy hadron/electron beam used by a number of different experiments. The new hyperon beam had to be designed allowing for a short changeover time between the different experiments and the different modes of operating H1.

- In addition to the H1 beam there are five more beams in the West Area complex operating at the same time. A hyperon beam always implies dumping a large number of protons close to the experiment, which creates an unavoidable muon background in the experimental hall. It was mandatory to reduce the muon flux to the neighbouring experiments as much as possible.

- The West Area, where the Omega spectrometer was located, is an open unshielded hall . It was necessary to cover more than 100 m of the H1 beam and in particular the surroundings of the hyperon production target with shielding. The maximum amount of shielding that could be installed without interfering too much with existing installations limited the proton flux to 5×10^{10} protons per pulse thereby imposing a limit on the intensity of the hyperon beam.

- Economically it was inconceivable to build any new beam line magnets and we thus had to rely upon those magnetic elements being available.

2.2 Basic design

The conditions listed above left little freedom in the basic design [5]. The first condition made a wobbling configuration a natural choice in order to preserve the direction of the H1 line and not to be forced to move the Omega spectrometer. The second condition suggested a bending of the beam in the vertical plane in order not to sweep the muons horizontally into other beam lines. Condition three together with the wanted Σ^- flux fixed the acceptance of the hyperon channel. The fourth condition limited the bending power available for the beam, the strongest bending magnets available being three H-type magnets, 3.6 meters long and each with a maximum field of 2.4 T.

At an early stage it was decided not to use any quadrupoles. This decision was dictated by space limitations and by the loss of intensity due to an increased beam length.

The choice of the beam momentum was a compromise between conflicting requirements. On the one hand, the Σ^-/π^- production ratio increases rapidly with the ratio of the hyperon beam momentum p_Y and the primary proton momentum, x_F $\approx \mathrm{p}_Y/\mathrm{p}_p$ with $\mathrm{p}_p = 450$ GeV/c , and the Σ^- decay losses are reduced by increasing p_Y. On the other hand, the Σ^- production cross section decreases rapidly with x_F as $\sigma \propto (1 - x_\mathrm{F})^3$. The limits on the primary proton flux mentioned above led us to the choice of $\mathrm{p}_c = 355$ GeV/c for the momentum on the central trajectory of the collimator, which corresponds to x_F = 0.8.

Fig. 1 shows the basic design of the beam line. The 450 GeV/c protons are incident from the left and bent down 7 mrad before interacting in the production target. Downstream of the target there were three 2.4 T magnets all filled with brass and tungsten collimators. A channel with small transverse dimensions was embedded in the tungsten defining the passage of the beam. The first magnet contained the dump region discussed below. The momentum spread of the beam was defined by the channel in the second magnet. The third magnet bent the beam back onto the geometrical axis of the Omega spectrometer.

2.3 Flux calculations

The Σ^- flux of the beam was estimated using the known π^--flux and measured values of the Σ^-/π^-ratio as a function of x_F (see Fig. 2). For the π^- flux we used measurements in the H1 and H8 beams both made at $x_\mathrm{F} = 0.8$. As the momentum bite of the beam is quite large the x_F dependence of the π^- flux also enters into the flux calculation. Here we assumed an x_F-dependence of the form $(1 - x_\mathrm{F})^4$. The result of the flux calculation as a function of the central momentum of the channel is shown in Fig. 3. The basic design is compared with a solution without wobbling. Also shown in figure 3 is the gain that would have been achieved with 3.0 T magnets had they been available. With these stronger magnets the required momentum spread of $\delta p/p = 15\%$ (FWHM) would have allowed for a larger angular acceptance of the magnetic channel and therefore an increased flux. This increase in flux is also seen in fig. 3. At the chosen value of the central momentum, $\mathrm{p}_c = 355$ GeV/c , the calculated Σ^-/π^- ratio was somewhat below 1. The design parameters of the beam are given in table 1.

3 Layout

3.1 Proton beam

The primary proton beam of the SPS with an energy of 450 GeV/c was extracted to the West Area in a slow extraction mode with a spill duration of 2.6 s and a cycle time of 14.4 s. The intensity was typically a few times 10^{12} protons per spill. A first intensity attenuation of the primary beam was provided by a production

target (T1). This 500 mm long Be target produced secondaries for the neighbouring H3 beam. A further reduction in intensity by roughly a factor 10 was obtained by a fixed hole collimator 20 m downstream of the T1 target. This collimator consisted of 4 iron blocks with transverse dimensions of 80 cm $\times$ 120 cm and with a length of 40 cm each in the direction of the beam. The blocks were equipped with tungsten inserts having small "pinholes" of diameter 3.3 mm. The fine tuning of the intensity was achieved by a movable four-jaw collimator located 35 m further downstream. It should be pointed out that the T1 target and the subsequent collimators were located in the horizontal plane of the accelerator ring i.e. some 20 m below the surface. This means that the muon background coming from the proton beam collimation is negligible at the surface, where the hyperon beam and the experiment were located.

The distance between the T1 target and the hyperon production target was approximately 800 meters. The protons were transported over this distance via the H1 beam line. This was a general purpose, high energy and high resolution beam (for details see [6]). The last 100 meters of the beam were modified in order to make space for the hyperon beam upstream of the Omega spectrometer.

The H1 beam line is equipped with MWPCs and scintillator filament scanners normally used for beam tuning . Obviously, those detectors could not be used for beam intensities of several 10^{10} protons per pulse. In order to tune the proton beam, attenuators consisting of 120 cm Be, i.e three interaction lengths, could be introduced just downstream of the T1 target. Together with the abovementioned four-jaw collimator this allowed to reduce the intensity down to the range of 10^7 protons per pulse suitable for tuning . Once the beam was tuned the absorbers were taken away and the collimators opened to obtain the full proton intensity on the hyperon production target. Several types of secondary emission monitors were installed just in front of the target in order to measure and monitor the proton flux and the position of the proton beam on the target. Fig. 4.a and 4.b show the horizontal and vertical profiles of the proton beam as measured with one of the secondary emission monitors just upstream of the target. The horizontal and vertical spot sizes were 250μm and 450μm, respectively (standard deviation). The divergence of the proton beam at the target was about 0.1 mrad horizontally and vertically.

3.2 Target choice

The target consisted of four Be rods each 100 mm long and 2 mm in diameter. The rods were suspended on thin aluminium foils ($25\mu m$) at each end. The target was motorized and could be moved in two orthogonal directions in a plane transverse to the beam. There is an interest to keep the diameter of the target as small as possible as long as the proton beam is well inside the target diameter. This minimizes secondary interactions which create low energy pions subsequently decaying into muons. The proton beam was well contained within the diameter of the target as can be seen from figures 4.a and 4.b . Beryllium was chosen as target material because the total inelastic cross section increases faster with A than the leading particle cross section. This means that, per interacting proton, the fraction of hyperons is largest for low A targets.

3.3 Magnetic channel

Fig. 5 shows the shape of the magnetic channel in both the bend and non-bend plane. Note that the horizontal axis is in meters and the vertical in cm. The channel is embedded in tungsten. Tungsten is chosen due to its very short interaction length thus stopping as many particles as possible before the decay.

The basic shape in both planes is a wedge opening towards the exit. Some tolerance has been added to take into account possible misalignments between successive magnets.

The shape of the first part of the channel is designed trying to minimise the muon background that originates from secondary pions and kaons created in the production target and decaying into muons before being absorbed in the walls of the channel. It turns out that the lateral dimensions are of small importance and what really matters is the longitudinal distance between the target and the dump. The distance can

however not be too small in order to ensure the necessary lateral separation between the Σ^--beam and the protons at the point where they are dumped. Taking this into account the distance was chosen to be 2.5 m.

In the more downstream part of the vertical section "pockets" have been added. The purpose of these pockets is to diminish the number of interactions in the walls and to trap part of the showers in the tungsten.

There is a disadvantage with the wobbling configuration of the beam as can be seen from the shape of the channel in the bend plane. Neutral particles can reach the exit of the channel from points far upstream in the channel. The geometry actually allows neutrals to escape from the channel from interactions in the walls starting at a distance of only 3.5 m from the production target. A local photon background was observed in the experiment at a place corresponding to an angle of 7 mrad above the beam. As can be seen from Fig. 5 this is consistent with the geometry of the channel. To confirm that this neutral background originates from the upstream part of the channel, 2 radiation lengths of lead were introduced between the second and the third magnets. This reduced the background by a factor 2-3. Moreover, if the production target is removed, the background disappears completely, showing that the background does not originate from the dump.

After the first beam period in 1998-90 the shape of the channel was partially modified to diminish this neutral background. The modifications are indicated in fig. 5. The second pocket was moved upstream and the walls were shaped in such a way that neutral particles from the target can not reach the upstream wall of the pocket which is seen by the exit and that the downstream part where neutral particles may hit the channel wall can not be seen from the exit. The point where the protons are dumped was also moved slightly upstream in order to preserve the distance between the dump and the second pocket to avoid any leakage into the pocket. The separation of the proton beam and the Σ^--beam at the dump was in this way reduced from 8 mm to 6 mm.

Fig. 6 shows a transversal cross section of the bending magnets. The pole gaps were filled with brass and tungsten collimators as mentioned previously. Each magnet had a fixed part and a removable part of inserts. The fixed part was made of brass for the two downstream magnets and of tungsten for the most upstream magnet. The removable part consisted of 90 tungsten block totally (30/magnet) with each block having its machined rectangular hole. The dimension of those blocks were 13 cm in the direction of the beam and 3.5×18 cm^2 transverse to the beam.

3.4 Detection and identification of beam particles

The beam momentum was measured with three hodoscopes, namely one scintillating fibre hodoscope placed before the last bending magnet and two sets of μ-strip silicon detectors located at two positions downstream of the magnetic channel (figure 1) A scintillating fibre hodoscope was chosen to allow the measurement of the particle position in the bending plane (z) with $250/\sqrt{(12)}\mu$m accuracy in the area of strong stray magnetic field and in the strong radiation environment of the magnetic channel.

The hodoscope was constructed of scintillating fibres (Kuraray SCSF-38) with rectangular cross section (1 x 0.5 mm^2). The fibres were covered by a 55 μm thick cladding to which a white pigment was mixed to prevent crosstalk. Three fibres were put together to form one channel (3×0.5 mm^2, figure 7). These three were glued to one clear fibre (1.5 mm $\times$ 1.5 mm $\times$ 1 m) as light guide which transmitted the light to one pixel of a 64-channel photo-multiplier. The channels were arranged in two rows which were displaced by half a fibre width (0.25 mm). The hodoscope had a total of 64 channels, 32 in each row. A valid hit was a coincidence between two fibres from each row. To prevent crosstalk at the tube causing wrong coincidences, neighbouring fibres were distributed over the 64 channels of the PM. Two such hodoscopes were used to obtain full efficiency.

At the exit of the beam channel the beam had to pass a hole of 5×5 cm^2 defined by a veto counter consisting of 2 cm lead sheets and 5 mm scintillator which was used to suppress the beam halo.

To reject high momentum π^- in the beam at an early stage of the trigger a fast transition radiation detector (TRD) was placed approximately 1 m downstream of the veto counter. This detector is described

in detail in [9]. Two scintillators each with an active area of 3.5×3.5 cm ^{2} in coincidence placed in front of the TRD and the experiments target were used to trigger on beam particles.

The trajectory of the beam particle in front of the experimental target was measured by a set of 8 high resolution silicon microstrip detectors with an active area of 5.1×5.1 cm^2 and with a pitch of 50 μm. A set of 4 planes was placed in front of the TRD detector, 4 planes were placed behind the TRD directly in front of the experiment target. The detectors measured in two orthogonal directions. The lower part of Figure 8 shows the setup around the experiment target.

Particles emerging from the interaction were detected in the WA89 spectrometer shown in the upper part of figure 8. The secondary particles close to the interaction point were detected by 20 silicon microstrip planes with 25 and 50μm pitch. Two scintillators (3.5×3.5 cm ^{2} each) were placed in the middle of the vertex detector to measure the multiplicity of particles coming from the interaction. These detectors were used in the trigger.

Positioning the target about 14 m upstream of the centre of the Ω-spectrometer provided a 10 m long decay area for short-living strange particles. The products of these decays along with the particles coming directly from the target were detected by 40 planes of drift chambers with a spatial resolution of about 300 μm. Special MWPC chambers (20 planes with 1mm wire spacing) were used in the central region of high particle fluxes. In order to improve the track matching between the target region and the decay region three sets of 4 MWPCs each with a pitch of 1 mm were installed about 2 m behind the target.

The particle momenta were measured by the Ω-spectrometer consisting of a super-conducting magnet with a field integral of 7.5 Tm and a tracking detector consisting of 45 MWPC planes inside the field area and 12 drift chamber planes at the exit of the magnet. The momentum resolution was $\sigma(p)/p^2 \approx 10^{-4}\ (\mathrm{GeV}/c)^{-1}$.

Charged particles were identified using a ring imaging Cherenkov (RICH) detector . It had a threshold of $\gamma = 42$ and provided π/p separation up to about 150 GeV/c. Downstream of the RICH a lead glass electromagnetic calorimeter was positioned for photon and electron detection . This calorimeter was followed by a hadron calorimeter. For a more detailed description see [10] and references therein.

4 Beam distributions

Figures 9.c and 9.d show the beam profile in horizontal (y) and vertical (z) direction at the position of the experiment target about 3 m from the exit of the beam channel. The beam had a width of 1.6 cm in y and a width of 3.7 cm in z direction. The shape of the beam profile in z reflects the momentum distribution of the beam. The beam profile in the non bending plane is a result of the profile of the proton beam and of the position of the beryllium target.

Figure 9a and b show the correlations between the beam particle impact point and its angle in the bending and non bending plane. All particle trajectories in the narrow bands in figure 9 point back to the production target. Particles outside the correlation bands are π^- from Σ^- decays, particles elastically scattered in the beam channel or muons. The distribution in figures 9a and 9.b were used to measure the amount of background in the beam from these sources (see below).

The momentum distribution of the beam was measured with the Ω spectrometer. For this measurement it was required that exactly one track was detected in the spectrometer to reject events with interactions. The momentum measurement for these non-interacting events was subsequently used to calibrate the beam hodoscope to be able to measure the beam particle momenta also for events where the Σ^- interacted in the target. The momentum distribution of beam particles for the 1994 data taking period is shown in figure 10. The solid line corresponds to the value measured by the beam hodoscope. The dashed line shows the momentum measurement in the spectrometer. This spectrum shows an additional component below 150 GeV/c stemming from the decays $\Sigma^- \rightarrow \mathrm{n}\pi^-$. The measurement of the beam momentum gave average

momenta of 345 GeV/c for the 1993 beam time and 330 GeV/c for the beam time in 1994 and a width of Δp/p = 18% (FWHM) which is close to the beam line design value of Δp/p = 15%.

5 Beam composition

5.1 Σ^- identification

In the TRD high momentum π^- were identified by their characteristic transition radiation, which was detected in ten double planes of multiwire proportional chambers. If three of the ten planes gave a signal above threshold the beam particle was identified as a high momentum pion and the event was subsequently rejected in the experiment trigger. The pulse height of each chamber was recorded for monitoring purposes and to allow a more detailed offline analysis at a later stage. Offline the pulse height information from the TRD chambers along the track measured in the the microstrip detectors was used to calculate a likelihood for the different particle hypotheses. The distribution of likelihoods for beam particles before and after the TRD decision is shown in fig. 11. From a two-component fit to the distribution of likelihoods before the TRD decision (fig 11.a) a Σ^-/π^- ratio of 0.38 ± 0.04 at the position of the TRD can be deduced, which is in very good agreement with the design value of the beam line. With the help of the TRD information the pion component for events in the experiment trigger was reduced to a Σ^-/π^- ratio of 10 ± 1 with a Σ^- detection efficiency of $82 \pm 1\%$ By a cut on the TRD likelihood in the offline analysis a Σ^- purity of 98.5 % was achieved while more than 95 % of the Σ^- identified online were retained.

5.2 Ξ^- in the beam

To measure the amount of Ξ^- in the beam, a sample of events with beam particles passing through the target without interaction was analysed. In this data sample we identified Σ^- and Ξ^- decays by the observation of decay kinks between the incoming beam particle and a negative particle detected in the spectrometer from the decays $\Sigma^- \rightarrow n\pi^-$ and $\Xi^- \rightarrow \Lambda\pi^-$, respectively. The decay lengths of Σ^- and Ξ^- at the same momentum differ by only 1% and therefore no acceptance or efficiency corrections are needed for a given fiducial volume to evaluate the Ξ^- / Σ^- ratio.

In part a) of fig. 12 the expected correlation (generated with the GEANT Monte Carlo) between momentum and kink angle for Σ^- and Ξ^- decays is shown. The experimental data for the correlation are displayed in fig. 12b. A second band originating from Ξ^- decays can be discerned there. For a quantitative analysis we projected this distribution along the angle-momentum correlation marked by the dashed and solid lines. This projection is shown by the solid histogram in part c) of fig. 12. Besides the dominating peak from Σ^- decays, a well separated maximum corresponding to Ξ^- decays can be identified. The observed distribution can be reproduced by Monte Carlo simulations assuming a Ξ^- contribution of (1.3 $\pm$ 0.1)% relative to the number of Σ^- (see cross-hatched histogram in fig. 12.c). This ratio is in good agreement with the numbers given in [8].

5.3 Ω^- and K^- in the beam

The production of Ω^- is expected to be even more suppressed than the production of Ξ^- due to the additional unit of strangeness. In figure 12b a sizeable contribution of Ω^- would be visible in a band above the correlation for Σ^- in the momentum range of 70-160 GeV/c . In this region of the plot no Ω^- can be identified above the background. The expected Ω^-/Ξ^- ratio at the channel exit calculated from the numbers given in [8] is 2×10^{-3} which is below the sensitivity of the measurement presented in figure 12.

The K^- component of the beam can be estimated on the basis of the K^- to π^- production ratio, which was measured to be $(1.15 \pm 0.02)\%$ [11] in 300 GeV/c p-Be collisions . Since the K^- are below the TRD

threshold they were not rejected by this detector. From the K^-/π^- ratio at production we deduce that there was a 2.1% admixture of K^- in the beam after the online rejection of the high-momentum π^- component.

5.4 Muon halo

There are two different origins of the muon background. One part comes from showers created by the protons being dumped in the tungsten. The second part is due to secondary pions and kaons created in the production target which decay into muons before being absorbed in the walls of the channel. The first kind of muon background is minimized by choosing a very dense material with a very short interaction length, such as tungsten. The second contribution depends on the geometry of the beginning of the channel as discussed in section 3.3. To obtain a rough idea of the muon background we have used the Monte-Carlo program HALO [12]. This program generates parent particles decaying into muons and the muons are then tracked through the coils and yokes of the different magnets. The result of this calculation is shown in table 2, where muon densities for 2×10^{10} protons are given at the entrance to the Omega spectrometer. Contributions from the dump and from the target have been separated. It can be seen that at the beam axis we expect about 2×10^5 muons/m^2 and that the dominating part comes from secondaries from the target.

The level of the muon background was measured with scintillator hodoscopes located a couple of meters downstream of the exit of the Omega spectrometer. About 2×10^5 muons/m^2 per pulse were measured, in good agreement with the calculations. Taking out the production target reduced this rate by a factor of 2.5, confirming the trends found in the calculations.

5.5 Backgrounds in the beam

The total amount of background in the beam can be estimated from the plots in figure 9. In this plots about 21 % of all measured particle trajectories do not fall into the angle-impact correlation which is given for particles coming from the production target. Of this 21 % about half could be assigned to π^- from Σ^- decays as shown by a Monte Carlo simulation of the beam line. The rest corresponds to muons and particles elastically scattered in the collimators.

To measure the effect of the veto counter data were taken in a special run where the veto counter was not included in the experiment trigger. Removing the veto counter resulted in an increase of 5 % of the multiplicity dependent part of the trigger rate. This increase was caused by additional particles crossing the apparatus together with the particles produced in the experiment target causing larger pulse heights in the multiplicity counters.

5.6 Interactions from Pions and Neutrons

With the given beam composition it was possible to obtain in addition to the events with Σ^- induced interactions data samples on interactions induced by π^- and neutrons:

To obtain a clean sample of events with pion interaction data was taken with an inverted TRD decision for a small fraction of the runing time. In this data sample the Σ^-component of the beam was suppressed online by the TRD to a level below 2 %.

For Σ^- decaying upstream of the centre of the last bending magnet the decay pion fell in the acceptance of the beam trigger counters. Since the momentum of the decay pion is below 150 GeV/c this events were not rejected by the TRD and were identified with the angle-impact correlation as mentioned above. In some fraction of this events however an interaction was induced by the decay neutron. It was possible to isolate a clean sample of such events by requiring that the beam particle trajectory was outside the angle-impact correlation and not pointing to the reconstructed interaction vertex. Additionaly it was required that the pion track could be followed into the spectrometer and had a momentum below 150 GeV/c.

Neutron and π^- induced interactions were used as control data sets to be able to compare to other experiments using these beams types [10].

6 Effect of the vertical target position

The vertical target position determined the position of the produced particles at the entrance of the magnetic channel and therefore the curvature of the central trajectory passing through the collimators of the magnetic channel. By moving the target up and down it was hence possible to tune the average beam momentum. For each given target position the proton beam could be steered onto the production target by means of a trimmer magnet.

The target position with maximum channel transmission was given by the geometrical acceptance of the collimator system. Since the Σ^-/π^- production ratio is strongly dependent on the average beam momentum this target steering also had an impact on the Σ^- content of the beam.

To find an optimal point of operation the target was moved $\pm$ 0.4 cm relative to its nominal zero position and the corresponding beam momenta and particle fluxes were measured. Figure 13 shows the results of these measurements. The average particle momentum varied from 310 to 360 GeV/c for this range of target positions (fig 13.a). The flux variation is shown in figure 13.b . At maximum transmission the flux was 5×10^5 particles (Σ^- and π^-) for 3.0×10^{10} incident protons. In 1993 the beam was operated with the target at position -0.05 which gave an average momentum of 345 GeV/c, a Σ^-/π^- ratio of 0.4 and a flux of 1.38×10^5 Σ^- particles at the channel exit.

7 Conclusions

A high-intensity double-bend hyperon beam was successfully operated at momenta between 330 and 345 GeV/c delivering 1.4×10^5 Σ^- to experiment WA89 in the CERN West Area. At the experiment target 3 m downstream of the channel exit the beam had a Σ^-/π^- ratio of 0.38 ± 0.04 and a size of 1.6 $\times$ 3.7 cm^2. The Ξ^-/Σ^- component of the beam was measured to be 1.3 ± 0.1 % in good agreement with previous measurements. The muon and neutral backgrounds were substantially reduced by a careful design of the proton beam dump area and the shape of the collimators. By an adjustment of the vertical target position it was possible to tune the beam momentum, the particle flux and the Σ^-/π^-ratio to an optimal value.

8 Acknowledgement

The members of the WA89 collaboration are grateful to the EA group for their continuous support in the construction and operation of the hyperon beam line, to the SPS staff for providing good beam conditions and to the Omega group for their help in running the Omega spectrometer. We would like to thank J. Zimmer for his invaluable support during all phases of detector development and setup.

References

[1] M. Bourquin and J.-P. Repellin, Physics Reports **114**,(1984) 99

[2] L. Pondrom, Physics Reports **122**,(1985) 57

[3] R. Edelstein et al., E781 proposal, Fermilab, 1987

[4] Proposal for a new hyperon beam experiment at the CERN-SPS using the Omega facility, CERN/SPSC-87/43,SPSC-P/233

[5] P. Grafström, A study of a high-energy Σ^- beam for the Omega spectrometer in the West Area. CERN/SPSC 88-4 and CERN/SL 90-104

[6] D.E.Plane, The West Area Beams CERN/SPS/83-22 (EBS)

[7] M.Bourquin et al.,Nucl.Phys. **B153**,(1979) 13

[8] T.R. Cardello et al., Phys. Rev **D32**, (1985) 1

[9] W. Brückner *et al.*, Nucl. Instrum. Methods **A378**, 451 (1996)

[10] M.I.Adamovich. *et al.*, Z.Phys. **C76**, 35-44 (1997)

[11] H.W.Atherton *et al.*, CERN 80-07, CERN, Geneva, Switzerland (1980)

[12] Ch.Iselin, HALO - A computer programme to calculate Muon Halo. CERN 74-17

Length of the beam from target to exit of channel (m)		12.7
B $\times$ l (Tm)		+17.2 ; -8.6
Deflection (mrad)		+13.8 ; -6.9
Central momentum (GeV/c)		355
Acceptance ($\pm 2\sigma$)	α_H (mrad)	± 1.5
	α_V (mrad)	± 0.6
	α_V (mrad)	± 12
Spot size at exit ($x \times y$ mm^2)		37×16
Flux of Σ^- for 3×10^{10} ppp		1.4×10^5
Σ^-/π^- ratio at channel exit		0.38 ± 0.04

Table 1: Parameters of the Σ^- beam

	Muons/m^2 at the beam axis over an area of 1×1m^2		Muons/m^2 0.85 m above (μ^-) and below (μ^+) the beam axis over an area of 0.3×0.3 m^2	
	μ^+	μ^-	μ^+	μ^-
From target	2.2×10^4	1.3×10^5	1.3×10^6	9.6×10^5
From dump	0.3×10^4	0.2×10^5	0.1×10^6	0.5×10^5
Total	2.5×10^4	1.5×10^5	1.4×10^6	1.0×10^6

Table 2: Calculated muons/m^2 at the entrance of the Omega spectrometer for 2×10^{10} incident protons

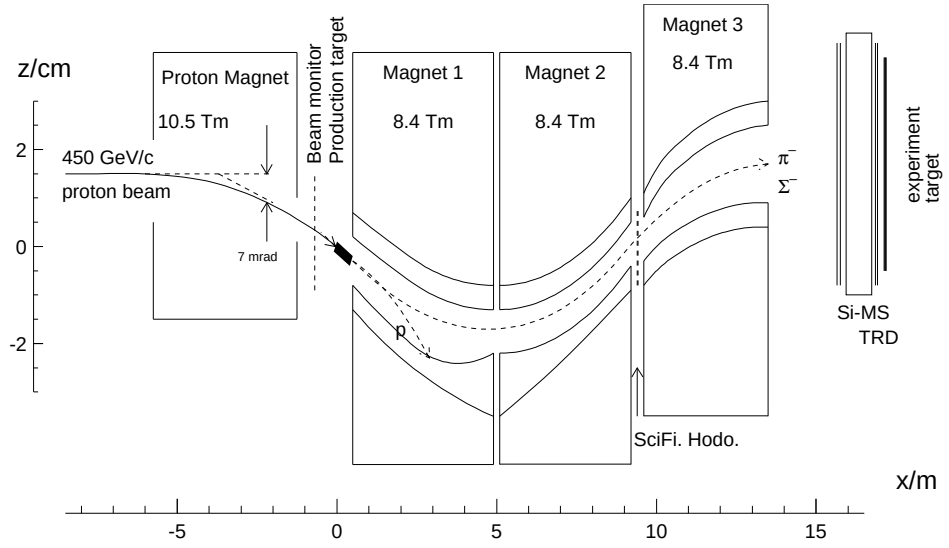

Figure 1: Basic layout of the hyperon beam channel and the target area of experiment WA89

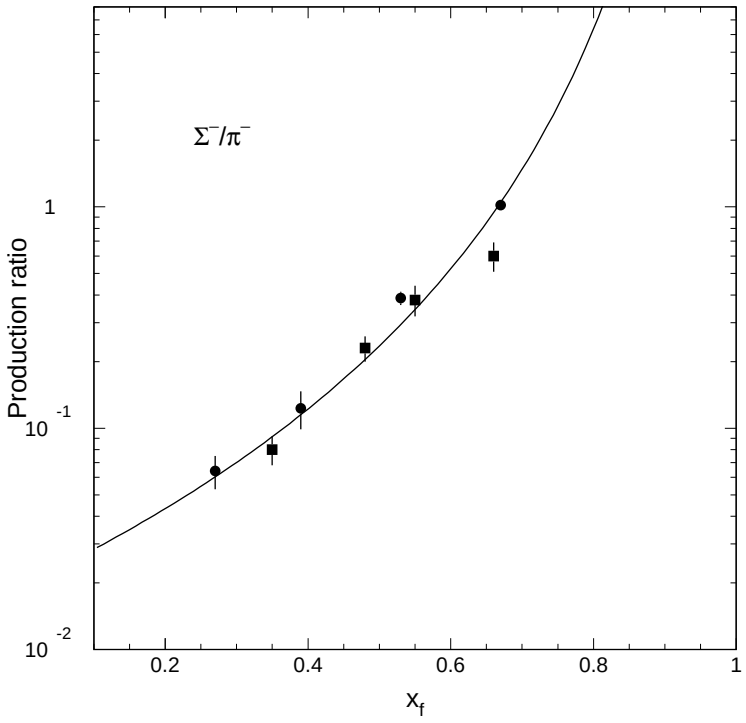

Figure 2: The Σ^-/π^-production ratio at small p_t as function of $x_{\rm F}$ (Solid squares from ref. [7]; Solid circles from ref. [8]). The solid line is a fit to the data at $p_t = 0$ given in [8].

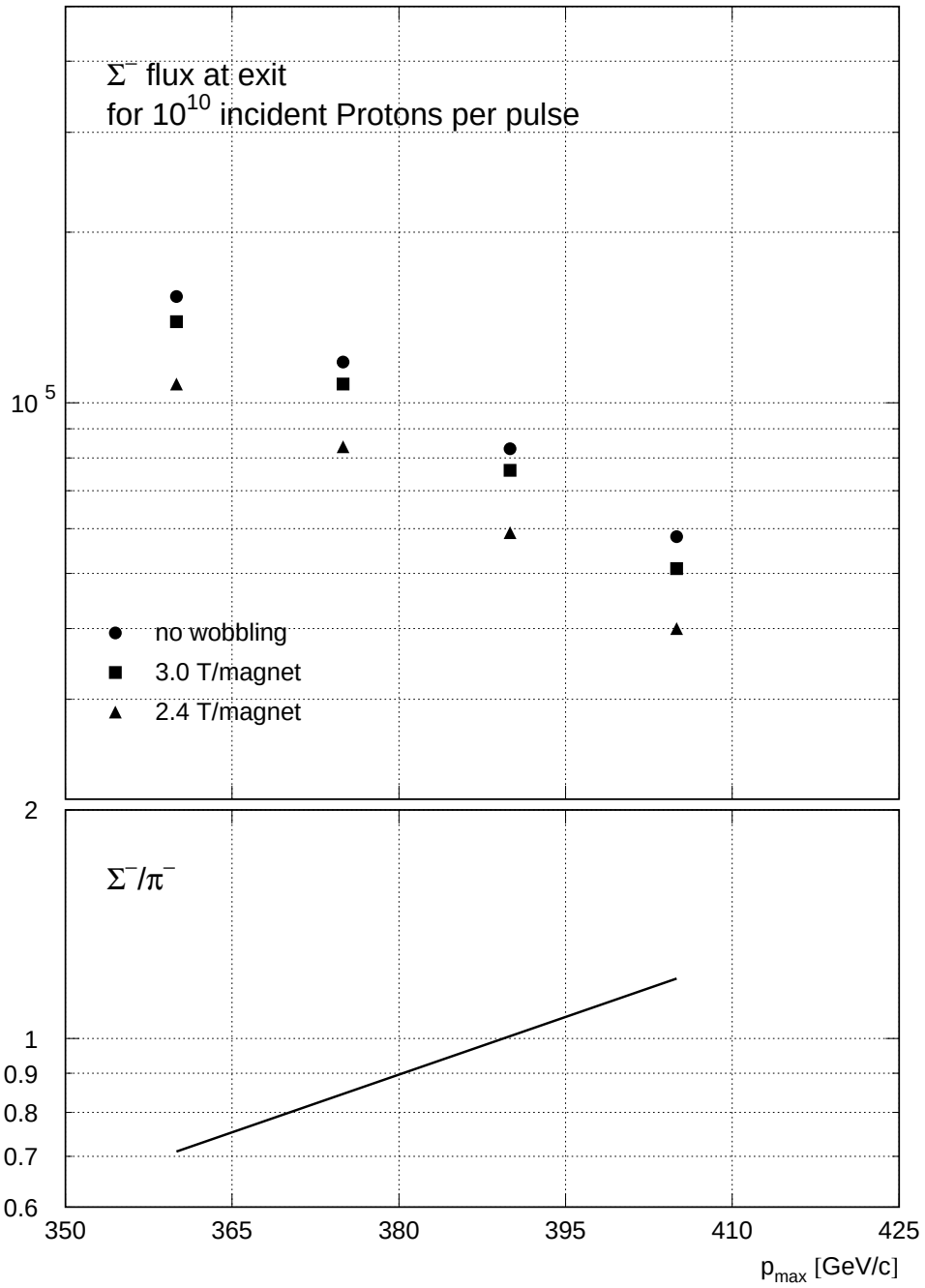

Figure 3: Σ^--flux for 2×10^{10} protons per pulse as a function of momentum of the central beam trajectory. All acceptances were adjusted to give $\Delta p/p = 15\%$ (FWHM)

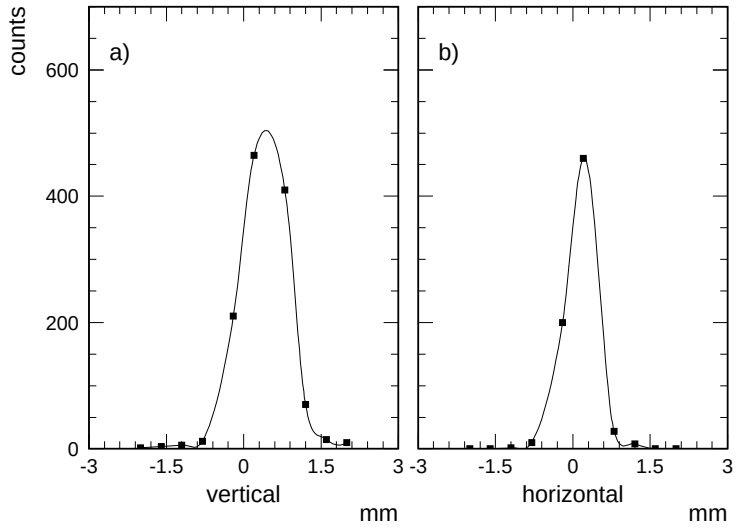

Figure 4: Vertical (a) and horizontal (b) beam profile of the proton beam at the production target

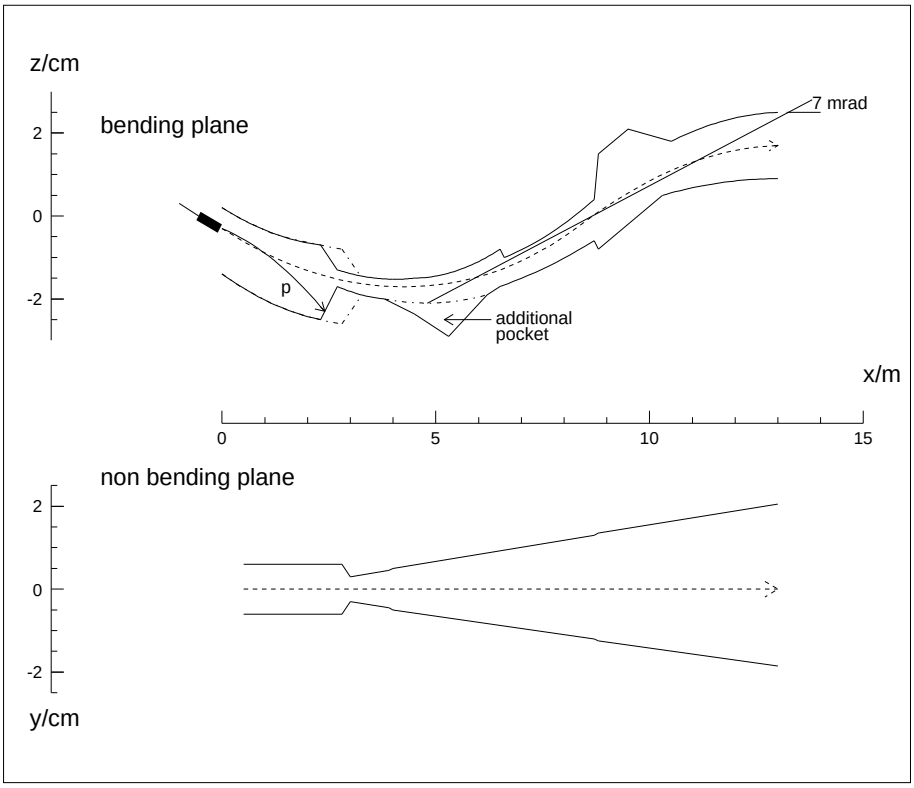

Figure 5: Shape of the tungsten channel in the horizontal and vertical plane. The dashed contours correspond to the pre-1991 setup

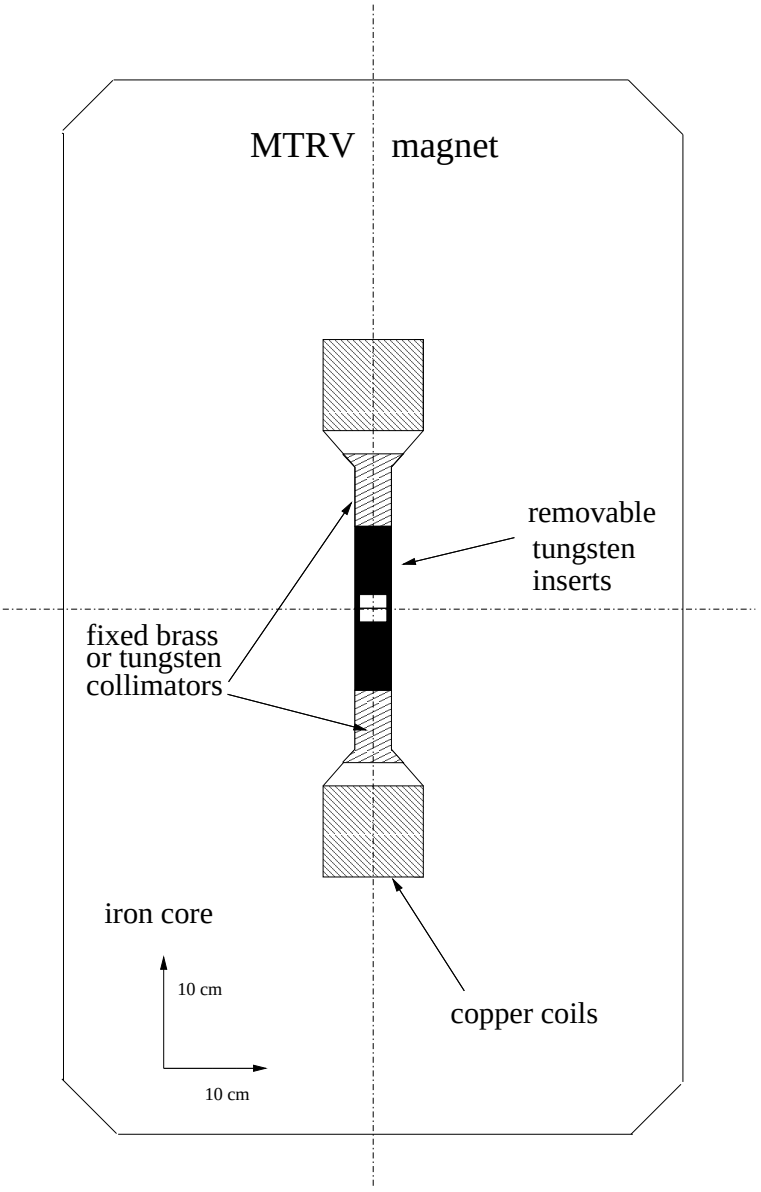

Figure 6: Transverse cross section of a bending magnet

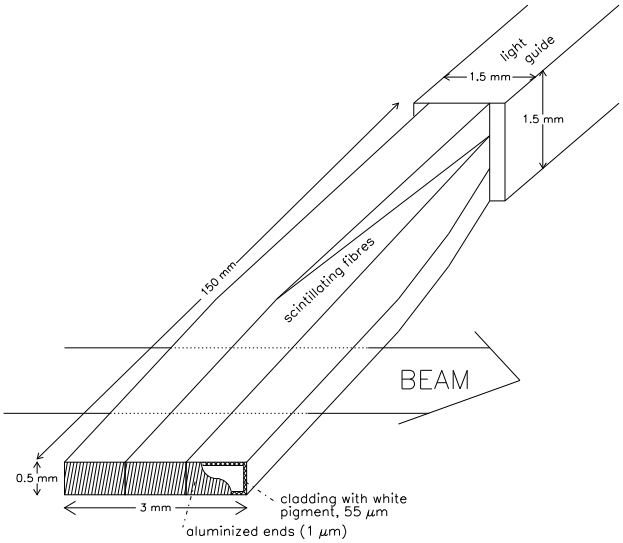

Figure 7: One channel of the beam hodoscope. The scintillating fibres were glued to a light guide (1 m long) which leads the photons to the PMT. The open ends of the scintillating fibres were aluminized to reflect the light emitted in the direction opposite to the light guide.

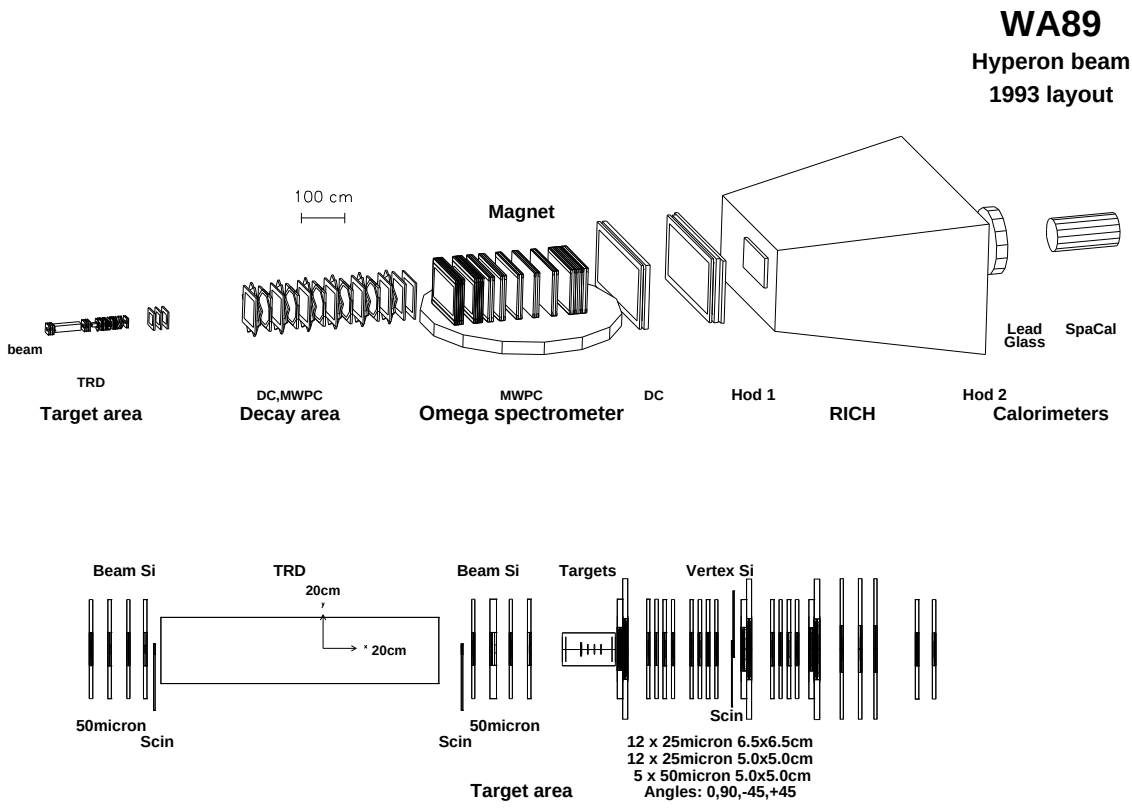

Figure 8: Setup of experiment WA89. The lower part shows the expanded view of the target area

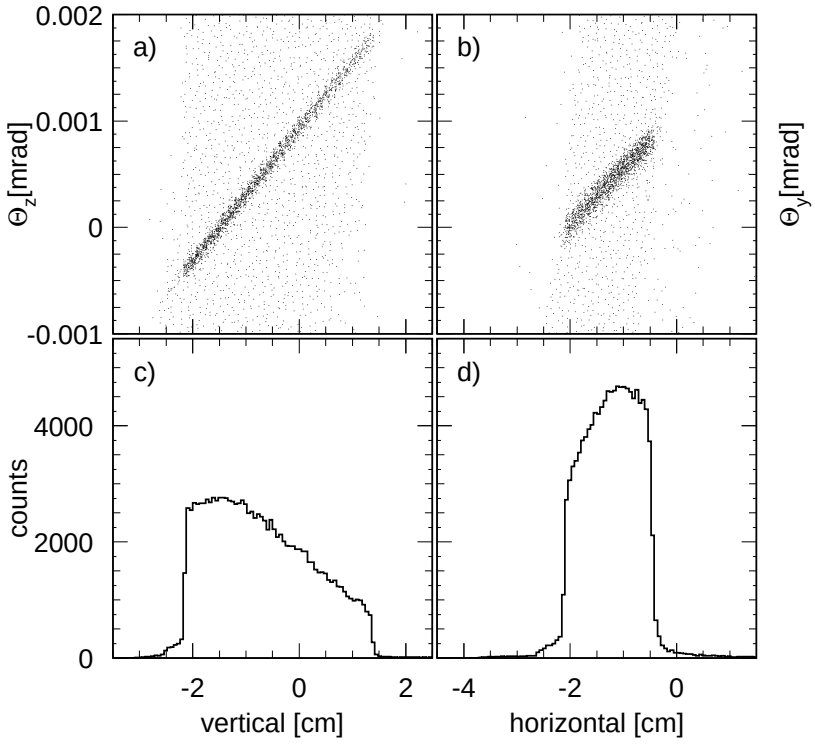

Figure 9: Angle-impact correlations (a and b) and beam profiles (c and d) at the experiment target $\sim$3 m downstream from the channel exit.

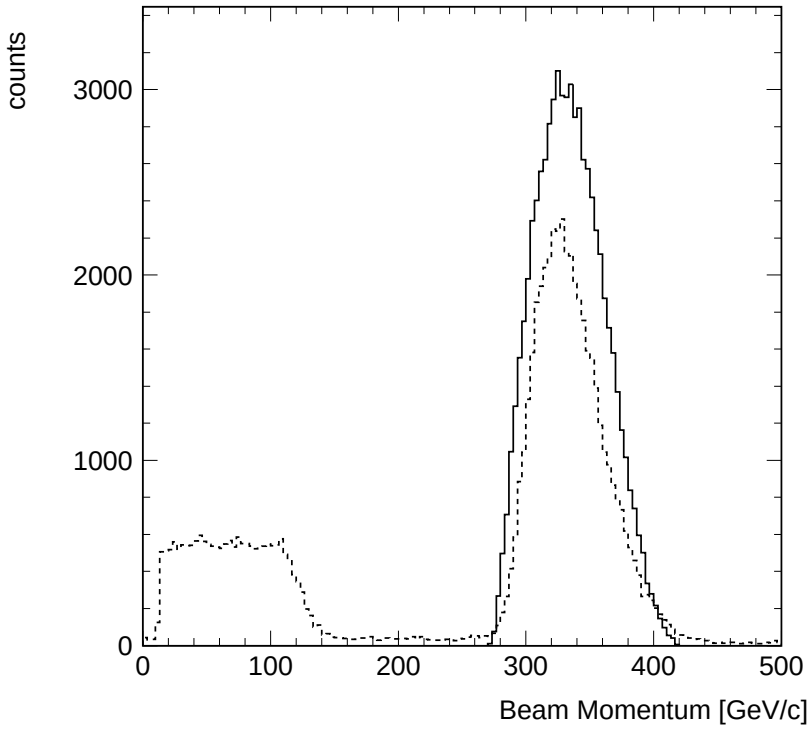

Figure 10: Beam momentum spectrum as measured with the beam hodoscope (solid line) and as measured in the Ω-Spectrometer (dashed line). The additional component below 150 GeV/c stems from decays $\Sigma^- \rightarrow \mathrm{n}\pi^-$(Data from 1994 beam time).

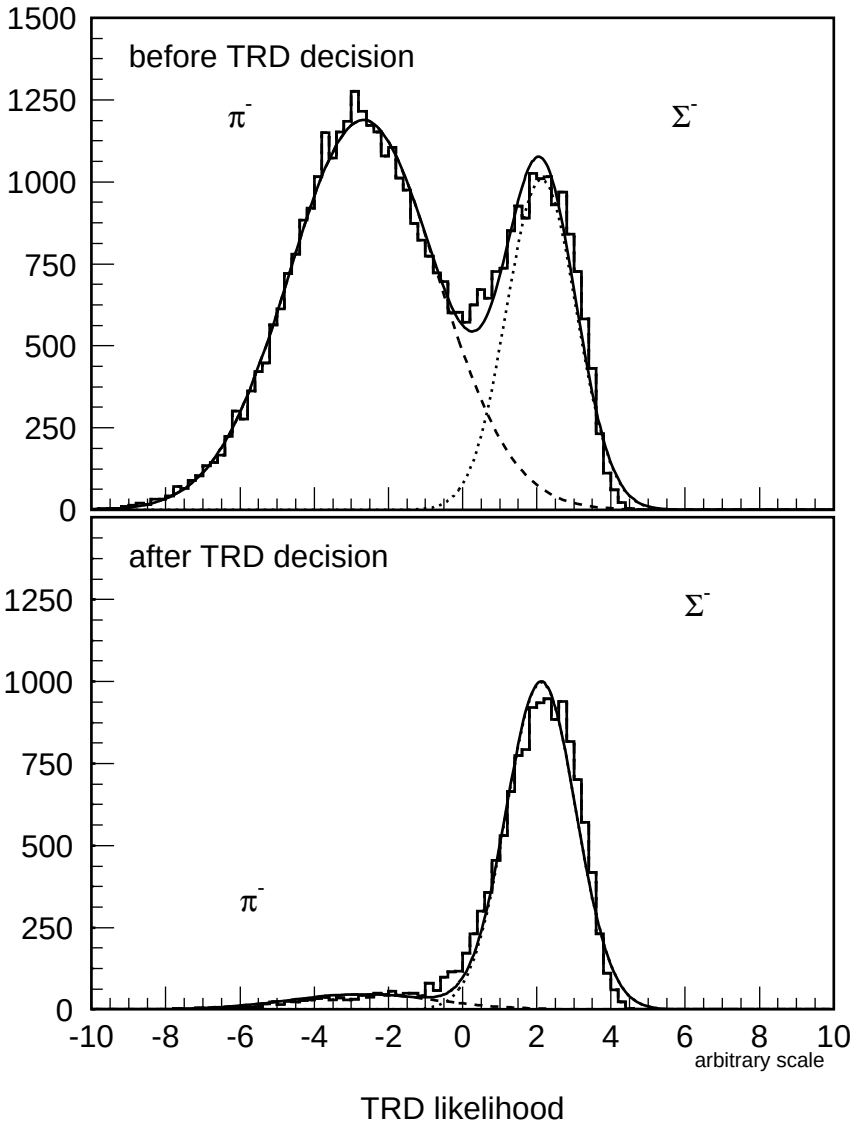

Figure 11: Distributions of TRD likelihoods before and after the TRD decision

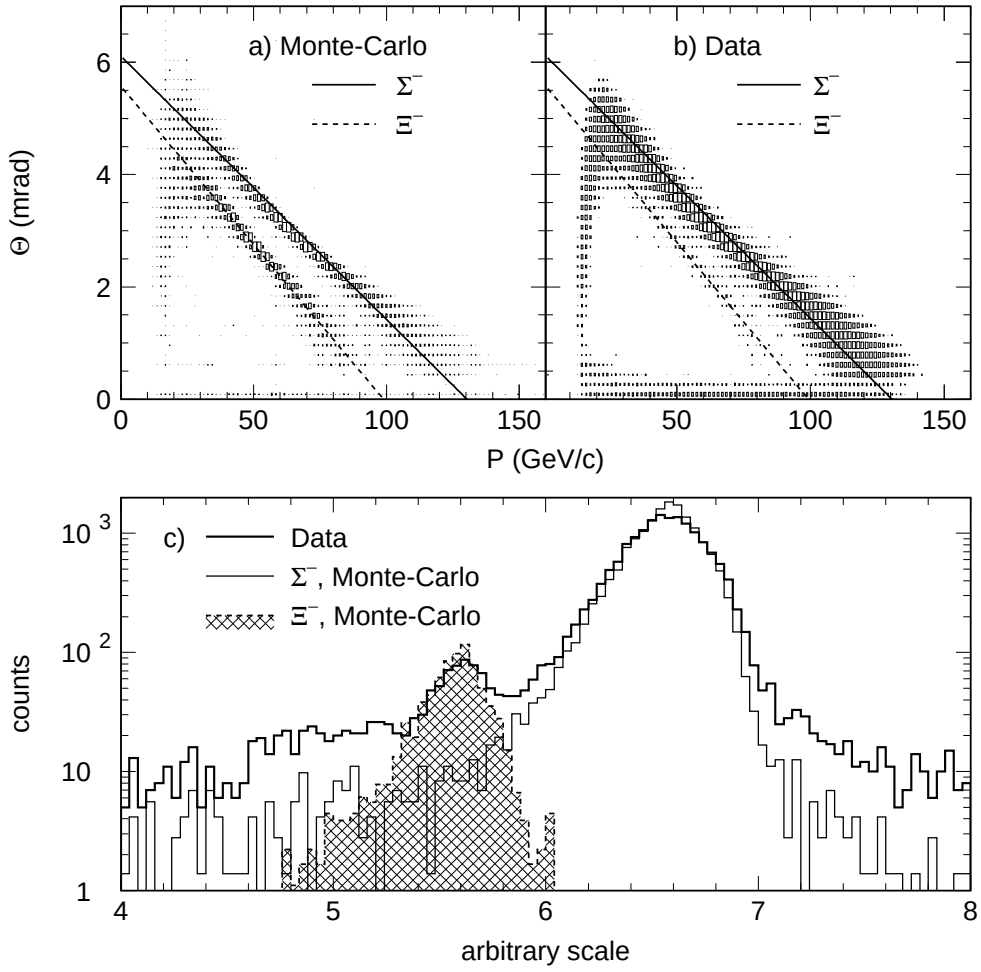

Figure 12: Correlation plots between momentum and decay angle between incoming Σ^- and Ξ^- and outgoing π^- for a) Monte Carlo and b) Data. The projections of these distributions along the two indicated lines are shown in part c). [10]

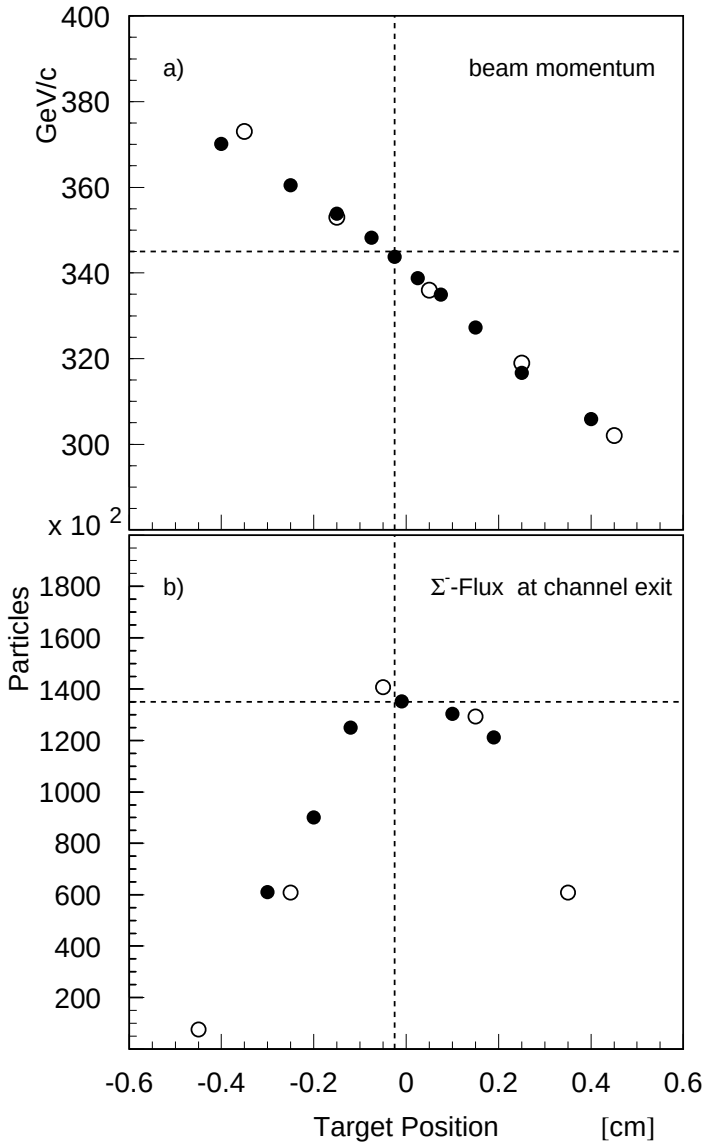

Figure 13: Beam momentum and particle flux as function of the target position. The solid points correspond to the measurements, the open points to the MC-calculation. The dashed lines indicate the working point of the hyperon beam channel in 1993.